THE JOURNAL OF BIOLOGICAL CHEMISTRY VOL. 288, NO. 37, pp. 26697–26708, September 13, 2013

SHANK3 Gene Mutations Associated with Autism Facilitate Ligand Binding to the Shank3 Ankyrin Repeat Region*

Received for publication, February 15, 2013, and in revised form, July 26, 2013 Published, JBC Papers in Press, July 29, 2013, DOI 10.1074/jbc.M112.424747

Marie Germaine Mameza[‡], Elena Dvoretskova[§], Margarete Bamann[‡], Hans-Hinrich Hönck[‡], Türkan Güler[‡], Tobias M. Boeckers[¶], Michael Schoen[¶], Chiara Verpelli[‖], Carlo Sala[‖], Igor Barsukov[‡‡], Alexander Dityatev[§ §§], and Hans-Jürgen Kreienkamp[‡1]**

*From the [‡]Institut für Humangenetik, Universitätskrankenhaus Hamburg-Eppendorf, Martinistrasse 52, 20246 Hamburg, Germany, the [§]Department of Neuroscience and Brain Technologies, Istituto Italiano di Tecnologia, Morego 30, 16163 Genova, Italy, the [¶]Institute of Anatomy and Cell Biology, Ulm University, 89081 Ulm, Germany, the [‖]Consiglio Nazionale delle Ricerche, Institute of Neuroscience and Department of Medical Biotechnology and Translational Medicine, University of Milan, 20129 Milano, Italy, the **Department of Neuromuscular Diseases and Neuroimmunology, Neurological Institute Foundation Carlo Besta, 20133 Milano, Italy, the [‡‡]Institute of Integrative Biology, University of Liverpool, Liverpool, Merseyside L69 3BX, United Kingdom, and the [§§]Molecular Neuroplasticity Group, Deutsches Zentrum für Neurodegenerative Erkrankungen, 39120 Magdeburg, Germany*

Background: Missense mutations in the *SHANK3* gene have been detected in autism patients.
Results: A mutation in the conserved SPN region of Shank3 improves ligand binding to the ankyrin repeats.
Conclusion: The SPN domain regulates accessibility of the ankyrin repeats through an intramolecular interaction.
Significance: Autism-associated mutations of Shank3 result in gain-of-function with respect to specific interaction partners.

Shank/ProSAP proteins are major scaffold proteins of the postsynaptic density; mutations in the human *SHANK3* gene are associated with intellectual disability or autism spectrum disorders. We have analyzed the functional relevance of several *SHANK3* missense mutations affecting the N-terminal portion of the protein by expression of wild-type and mutant Shank3 in cultured neurons and by binding assays in heterologous cells. Postsynaptic targeting of recombinant Shank3 was unaltered. In electrophysiological experiments, both wild-type and L68P mutant forms of Shank3 were equally effective in restoring synaptic function after knockdown of endogenous Shank3. We observed that several mutations affected binding to interaction partners of the Shank3 ankyrin repeat region. One of these mutations, L68P, improved binding to both ligands. Leu-68 is located N-terminal to the ankyrin repeats, in a highly conserved region that we identify here as a novel domain termed the Shank/ProSAP N-terminal (SPN) domain. We show that the SPN domain interacts with the ankyrin repeats in an intramolecular manner, thereby restricting access of either Sharpin or α-fodrin. The L68P mutation disrupts this blockade, thus exposing the Shank3 ankyrin repeat region to its ligands. Our data identify a new type of regulation of Shank proteins and suggest that mutations in the *SHANK3* gene do not necessarily induce a loss of function, but may represent a gain of function with respect to specific interaction partners.

Autism spectrum disorders (ASDs)[2] are characterized by delayed acquisition of speech, deficits in social communication, and stereotypic behaviors. The analysis of genetic causes for ASD has recently uncovered mutations in genes coding for several synaptic proteins, pointing to a synaptic cause of the disease. Mutated genes include those coding for the synaptic adhesion molecules Neurexin (1) and Neuroligin (2), as well as postsynaptic scaffold proteins Shank3/ProSAP2, Shank2/ProSAP1, and more recently Shank1 (3–5). In the case of Shank proteins, several of the genomic alterations observed in patients lead to a loss of function for one copy of the gene. In addition, a number of rare missense mutations have been identified in autistic patients which are not likely to be causative for the disease but may constitute strong risk factors (3, 5, 6).

Shank/ProSAP proteins are major scaffold proteins of the postsynaptic density (PSD) of excitatory (glutamatergic) synapses in the central nervous system (7–9). Via conserved protein interaction motifs (ankyrin repeats, SH3 and PDZ domains, a proline-rich region and a sterile alpha motif (SAM)), they bind to other components of the PSD and are involved in the generation of dendritic spines and in the postsynaptic specialization (10–12). To date, it is unclear how individual missense mutations affect Shank3 function, in particular as all patients identified so far are heterozygous for the mutations. ASD-related mutations are in most cases not localized to known functional domains or interaction motifs of the protein;

* This work was supported by Deutsche Forschungsgemeinschaft Grants FOR885, IRP2, and Kr1312/3–2 (to H.-J. K.), Telethon Fondazione Onlus Grant GGP11095 (to C. S. and A. D.), Istituto Italiano di Tecnologia (to A. D.) and Seed grant (to C. S.), Ministry of Health in the frame of European Research Area Network NEURON (to C. S.), and Programma Nazionale per la Ricerca-Consiglio Nazionale delle Ricerche Aging Program 2012–2014 (to C. S.).

[1] To whom correspondence should be addressed. Tel.: 49-40-74105-4395; Fax: 49-40-74105-5138; E-mail: Kreienkamp@uke.de.

[2] The abbreviations used are: ASD, autism spectrum disorder; ANOVA, analysis of variance; ARR, ankyrin repeat region; DIV, days *in vitro*; GKAP/SAPAP, guanylate kinase-associated protein/synapse-associated protein (SAP)-associated protein; mEPSC, miniature excitatory postsynaptic current; mRFP, monomeric red fluorescent protein; PDZ domain, domain found in PSD-95/discs large/ZO-1; ProSAP, proline-rich synapse-associated protein; PSD, postsynaptic density; SH3 domain, Src homology 3 domain; Shank, SH3 and ankyrin repeat-containing; SPN domain, Shank/ProSAP N-terminal domain; SUMO, small ubiquitin like modifier.

therefore it is difficult to predict whether any particular function of Shank3 may be disrupted. Expression of some mutant forms of Shank3 (R12C, R300C and Q321R) in neurons leads to changes in spine morphology, most likely via an actin polymerization-dependent mechanism (13). Interestingly, several mutations have been localized to the ankyrin repeat region (ARR) and to a highly conserved N-terminal region (termed Shank/ProSAP N terminus or SPN here) of approximately 90 amino acids which immediately precedes the ARR (3, 6). Due to alternative splicing and differential promoter usage, not all expressed Shank variants contain the N-terminal SPN and ARR domains; thus in the forebrain, both Shank1 and Shank3 contain these two domains, whereas Shank2 does not (14). Whereas the SPN region has so far remained functionally uncharacterized, the ARR is known to interact with the cytoskeletal protein α-fodrin (15) and with Sharpin (16). Sharpin is involved in NFκB and integrin-dependent signaling pathways (17–21), but its role in the nervous system has not yet been characterized. Here, we analyzed the impact of mutations in the SPN and ARR on functional properties of the Shank3 protein. We found that several mutations in the ARR, and surprisingly also in the SPN region, improved binding of the ARR to Sharpin as well as α-fodrin. Our data identify the SPN sequence as a new functional domain of Shank proteins. By binding to the ARR domain, it has a regulatory function with respect to ARR ligands. In addition, our data show that heterozygous missense mutations may lead to a gain of function with respect to interaction with Shank3-associated proteins.

EXPERIMENTAL PROCEDURES

Expression Vectors—The rat Shank3 cDNA (accession number AJ133120) in the expression vector pcDNA3.1myc/his has been described; it leads to expression of full-length Shank3 carrying a C-terminal myc tag (22). For site-directed mutagenesis, a 1.3-kb EcoRV fragment encompassing the 5′ end of the cDNA was subcloned into pBluescript, and mutations were introduced using the QuikChange II Site-directed mutagenesis kit (Stratagene). Mutant fragments were sequence-verified by dideoxy sequencing and reintroduced into the full-length expression vector via the EcoRV sites.

For lentivirus-based RNA interference, Shank3 oligonucleotides were annealed and inserted into the HindIII/BglII sites of the pLVTHM vector for lentivirus production. We used siRNA sequences targeted against a sequence that is identical in rat and mouse Shank3 mRNA: 5′-GGAAGTCACCAGAGGACAAGA-3′. To make Shank3 expression constructs resistant to shRNA, further silent mutations were introduced into the recognition region for the shRNA (changing it to 5′-GGAAATCGCCGGAAGATAAA-3′; altered bases underlined).

mRFP-tagged deletion constructs of Shank3 were based on pmRFP-C1 (23). The mRFP coding sequence for the vector construction was obtained from Prof. Roger Tsien (University of California at San Diego, La Jolla, CA; see Ref. 24). WT and L68P mutant Shank3 fragments were introduced into pmRFP-C1 by taking advantage of restriction sites in the Shank3 coding sequence. A cDNA fragment containing bp 6043–7795 of the α-fodrin cDNA (accession number BC070885; see Ref. 15) was cloned into pEGFP-C3 (Clontech). The rat Sharpin cDNA was obtained from Eunjoon Kim (KAIST, South Korea) and cloned into pEGFP-C3. The cDNA fragment coding for the SPN region of rat Shank3 was cloned into pEGFP-C1.

Tissue Culture, Transfections, and Precipitation Assays—Human embryonic kidney cells (HEK293) were grown in DMEM containing 10% fetal bovine serum and transfected using Turbofect (Fermentas, Vilnius, Lithuania) according to the manufacturer's instructions. For the precipitation of Shank3, GKAP-Sepharose was prepared by coupling a synthetic peptide corresponding to the 10 C-terminal residues of GKAP/SAPAP1 (NH_2-IYIPEAQRTL-COOH; custom synthesized by EZBiolab Inc. Westfield, IN) to NHS-Sepharose (GE Healthcare) at a concentration of 3 mg/ml matrix. For precipitation of GFP or mRFP fusion proteins, GFP-trap or mRFP-trap matrices were obtained from Chromotek, Munich, Germany. Transfected cells were lysed in radioimmune precipitation assay buffer (50 mM Tris-HCl, pH 8.0, 150 mM NaCl, 1% Nonidet P-40, 0.5% sodium deoxycholate, 5 mM EDTA, 0.1% SDS, 0.2 mM phenylmethylsulfonyl fluoride, 1 μg/ml pepstatin, 10 μg/ml leupeptin) and centrifuged for 20 min at 20,000 × *g*. Clear supernatants were incubated with either GKAP-Sepharose, mRFP-trap, or GFP-trap for 2 h at 4 °C. Beads were sedimented by centrifugation at 1000 × g for 5 min, and washed four times with radioimmune precipitation assay buffer. Aliquots of input and precipitate samples were analyzed by Western blotting using appropriate antibodies (rabbit α-Shank PDZ (25); mouse α-GFP (Covance); rabbit α-mRFP (23); rabbit α-Sharpin (custom immunization using a GST-Sharpin fusion protein by Biogenes GmbH, Berlin, Germany). Chemiluminescent Western blot signals were quantified by a ChemiDoc XRS luminescence imager (Bio-Rad) in combination with Quantity One software.

Hippocampal neurons were prepared at embryonic day 19 and plated at a density of approximately 500 cells/mm^2. Cultures were grown in Neurobasal medium (Invitrogen) supplemented with B27 (Invitrogen) and 0.5 mM glutamine. 12.5 μM glutamate was included for the first 4 days in culture. Cells were transfected with full-length WT or mutant Shank3 expression vectors at day 8 *in vitro* (DIV8) using Lipofectamine 2000 (Invitrogen). For immunocytochemistry, neurons were fixed at DIV13 with 4% paraformaldehyde in PBS and permeabilized with 0.1% Triton X-100 in PBS for 5 min at room temperature. After blocking (2% horse serum in PBS) for 1 h at room temperature, cells were incubated with mouse anti-myc antibody (Sigma; diluted 1:1000 in blocking solution) and rabbit anti-MAP2 (obtained from Craig Garner, Stanford, CA; 1:5000) for 2 h at room temperature, followed by 1 h of incubation with Cy3-conjugated anti-mouse and Alexa Fluor 488 anti-rabbit (diluted 1:400 in blocking solution). Immunostaining was visualized by fluorescence microscopy using a Leica DMIRE2 confocal microscope. Images acquired with the 60×objective and GFP- and mRFP-specific filter settings were processed using Paintshop Pro software.

Yeast Two-hybrid Screen—A cDNA fragment coding for residues 1–103 of the human Shank1 protein (bp 233–541, accession number NM_016148) was cloned into the two-hybrid bait vector pGBKT7 (Clontech) in-frame with the Gal4 DNA binding domain. This bait plasmid was transformed into yeast strain AH109; the resulting strain was mated with the Y187 strain

carrying a pretransformed Matchmaker human brain cDNA library (Clontech) according to the manufacturer's protocols. Positive clones were selected by growth on the respective dropout media, and analyzed for β-galactosidase activity. After plasmid isolation, positive clones were subjected to retransformation into yeast cells together with bait and control plasmids (to verify specific interaction) and subsequently sequenced.

Cell Cultures for Patch Clamp Recordings—Primary murine hippocampal neuronal cultures were prepared as described previously (26). Hippocampi from 1–3-day-old C57BL/6J pups were dissected at 4 °C, and the neurons were recovered by enzymatic digestion with trypsin and mechanical dissociation. Cells were then plated at a density of 300/mm^2 in Neurobasal-A medium supplemented with 5 μg/ml gentamycin, 2% B27 supplement, 25 ng/ml FGF2, and 0.5 mM L-glutamine (all from Invitrogen) on 18-mm glass coverslips (Menzel-Glaser) coated overnight with 100 μg/ml poly-L-lysine (Sigma-Aldrich) and 40 μg/ml laminin (Sigma-Aldrich). Cultures were maintained at 37 °C in a 95% O_2, 5% CO_2 humidified incubator. From the 3rd day in culture, the medium was supplemented with 0.5 μM AraC (Sigma-Aldrich) to prevent glial cell proliferation. The medium was changed twice a week.

Infection and Transfection of Neurons—Primary hippocampal neurons were infected on DIV6–8 with lentiviruses expressing GFP (shCtrl) or GFP plus shRNA (shShank3) to knock down expression of Shank3. Infected neurons were transfected on DIV11 with pcDNA3 (mock) or with WT or the L68P mutant form of Shank3. A vector expressing the red fluorescent protein tdTomato was co-transfected in these experiments to identify transfected neurons. A modification of the calcium phosphate precipitation method was used for transfection (27). Briefly, neuronal cultures were incubated with the DNA-calcium phosphate precipitate for ~1.5 h. After incubation, the precipitate was dissolved by incubation for 15 min in a medium that had been preequilibrated in a 10% CO_2 incubator. The plates were then returned to their original conditioned medium and checked the next day for tdTomato expression. Cells were used for electrophysiological recordings 3–4 days after transfection.

Whole Cell Recordings from Hippocampal Cultures—Whole cell recordings from pyramidal-like neurons were obtained as described previously (28). Electrodes with a resistance in the range of 3–6 megohms were filled with a solution that contained 130 mM $CsMeSO_4$, 8 mM NaCl, 4 mM Mg-ATP, 0.3 mM sodium GTP, 0.5 mM EGTA, and 10 mM HEPES, pH 7.25. Cells were perfused continuously with HEPES-buffered saline of the following composition: 119 mM NaCl, 5 mM KCl, 2 mM $CaCl_2$, 2 mM $MgCl_2$, 25 mM HEPES, 33 mM D-glucose, 0.0005 mM tetrodotoxin citrate (Tocris), and 0.05 mM picrotoxin (Tocris), pH 7.35. The osmolarity of HEPES-buffered saline was adjusted to that of the culture medium on the day of recording. The osmolarity of the electrode solution was 10 mosM less than that of HEPES-buffered saline. Data were digitized at 10 kHz. Continuous recording of miniature EPSCs (mEPSCs) was made using an EPC10 USB patch clamp amplifier and PATCHMASTER software (HEKA Elektronik). Detection and measurements of mEPSCs, which were collected over a 3-min period, were performed using MiniAnalysis software (Synaptosoft, Leonia, NJ) after filtering of traces at 1 kHz and using a detection threshold of 6 pA (*i.e.* above 4× the S.D. of base-line noise) and visual verification of all detected events. Only cells with leak current < -100 pA were analyzed.

Statistical Analysis—For immunoprecipitation data, the blot signal of the precipitated protein was first normalized to the intensity of the respective input signal. This was then compared with the ratio obtained with the wild-type protein. For comparisons of multiple mutants, ANOVA, followed by Dunnett's correction for multiple comparisons was used. For comparing single mutants with WT, a paired Student's *t* test was used. Statistical analysis was performed on the raw data, whereas data normalized on wild type (or on the L68P mutant in one figure) are shown in the figures. For electrophysiological data, ANOVA on ranks was used in combination with Dunn's *t* test for multiple comparisons.

Structural Analyses—Secondary structure predictions were performed at Network Protein Sequence Analysis using default parameters (29). For expression of Shank3 fusion proteins, cDNAs coding for fragments of Shank3 were cloned into Champion™ pET SUMO vector (Invitrogen) and expressed in *Escherichia coli* BL21 Star (DE3) cultured in LB. Protein was purified by immobilized metal-affinity chromatography and gel filtration after the removal of the SUMO tag. NMR samples were prepared at 2 mg/ml protein concentration in 20 mM sodium phosphate, pH 6.5, 150 mM NaCl buffer with 5% ^2H_2O. Spectra were collected on Bruker AVANCE II+ 800 MHz spectrometer equipped with CryoProbe at 298 K.

RESULTS

Normal Synaptic Targeting of Mutant Shank3 Proteins—We introduced several of the mutations found in autism patients into a cDNA expression vector coding for a myc-tagged version of the rat Shank3 protein. We focused on amino acid exchanges in the N-terminal part of the protein (L68P, R300C, and Q321R; see Fig. 1*A*). Initially, we analyzed whether these mutations affect the postsynaptic targeting of Shank3 in cultured hippocampal neurons. Primary neurons were transfected on DIV7 and fixed and processed for immunocytochemistry on DIV14. WT Shank3 and all three mutants tested were found in a punctate manner along dendrites of transfected neurons. Costaining with the dendritic marker MAP2 revealed that these puncta are mostly localized on dendritic spines emanating from the main dendritic shaft (Fig. 1*B*). Quantitation of fluorescence intensities showed that the ratio of spine signal *versus* signal in the adjacent dendritic shaft does not differ for WT and mutant Shank3 forms, indicating that postsynaptic targeting is intact for all three mutant forms of Shank3 tested (Fig. 1*C*). Further costaining with an antibody against the vesicular glutamate transporter (vGlut; a marker for glutamatergic axon terminals) confirmed that Shank3-positive punctae are found in close proximity to presynaptic terminals (Fig. 2*A*). Quantitation of the number of Shank3-positive spines showed equal numbers of spines for the WT and all three mutants, revealing no difference in the ability of Shank3 variants to induce the formation of dendritic spines (Fig. 2*B*).

To gain insight into the role of mutated Shank3 in synapse formation and function, we knocked down Shank3 in hip-

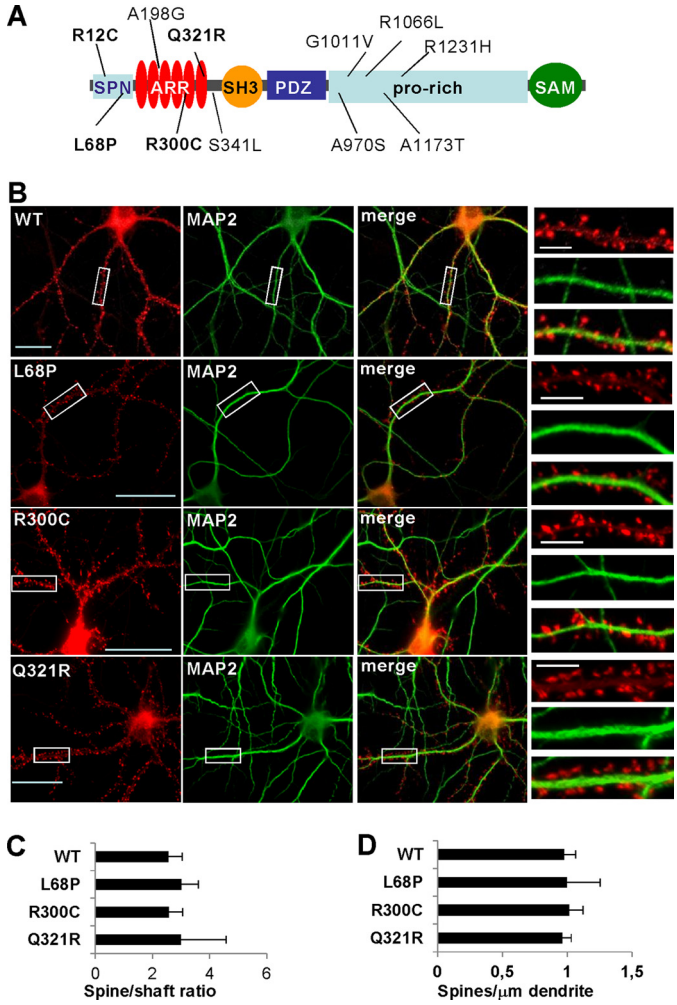

FIGURE 1. **ASD mutations in Shank3 do not affect localization on dendritic spines in cultured hippocampal neurons.** *A*, overview of the domain structure of the Shank3 protein. The positions of individual point mutations found in ASD patients are indicated. Mutations analyzed in this paper are indicated in *bold print*. Please note that the rat Shank3 mRNA (database entry AJ133120.1) contains two translational start sites, which lead to protein products differing in length by 75 amino acids. The numbering of amino acids in this paper refers to the shorter variant (generated from the more 3′ located start site), as it is consistent with the numbering for human Shank3 (also see below, Fig. 4). *SAM,* sterile alpha motif. *B*, WT and mutant Shank3 expression vectors carrying a C-terminal myc tag were transfected into primary cultured hippocampal neurons. Five days after transfection (DIV13) neurons were fixed and stained using anti-myc (Shank3; *red fluorescence*) and anti-MAP2 (a marker for neuronal dendrites, *green fluorescence*). Cells were visualized using confocal microscopy. Dendritic segments indicated by *white rectangles* are shown in higher magnification. *Scale bars*, 20 μm, 4 μm in magnified pictures. *C*, targeting of overexpressed Shank3 to dendritic spines. Fluorescence intensities in spines and the adjacent dendritic shafts were quantified using ImageJ. Data are represented as the spine/shaft intensity ratios ± S.D. 180 spines from nine cells derived from three or four independent experiments were evaluated. *D*, dendritic segments evaluated for the number of Shank3-immunopositive spines. Data are represented as the number of spines per μm of dendrite (±S.D.). For each mutant, 27 segments from nine cells derived from three or four independent experiments were evaluated. The evaluating person was blind to the experimental condition.

pocampal neurons using RNA interference. Shank3-specific shRNA (shShank3) or a control shRNA (shCtrl) was expressed via infection with lentiviral vectors. WT or L68P mutant Shank3 was then reintroduced by transfection, and transfected cells were identified by coexpressed mRFP. Recording of mEPSCs in pyramidal-like GFP-expressing neurons in shShank3- and shCtrl-treated cultures revealed that knockdown of Shank3 expression strongly reduced the frequency of mEPSCs; however, neither their amplitude nor their time course was affected (Fig. 2, *C* and *D*). The observed reduction in mEPSC frequency in shShank3-treated cultures is consistent with the reported increase in mEPSC frequency when Shank3 is overexpressed in aspiny cerebellar neurons (11). The reduction in the mEPSC frequency in shShank3-treated cultures could be reversed by transfection with a shShank3-resistant form of WT Shank3 (Fig. 2, *C* and *D*), confirming the specificity of the shShank3 knockdown and subsequent effect on the mEPSC frequency. Transfection of shShank3 treated neurons with the L68P mutant form of Shank3 also fully restored the frequency of mEPSCs to control levels. The amplitude and shape of mEPSPs were also not affected by the mutation (Fig. 2*D*), suggesting that the L68P mutant supports normal excitatory synaptic transmission and does not result in a loss of function. Efficient knockdown of Shank3 by the Shank3 shRNA to approximately 20% of control levels was confirmed by Western blotting (Fig. 2*E*). The level of other Shank family members remained unaffected; the selectivity and efficiency of this procedure have been described before (30).

ASD Mutations Affect Binding of the ARR Domain—We analyzed whether the mutations affect binding to known interaction partners of Shank proteins. The ARR domains of both Shank3 and Shank1 bind to the cytoskeletal protein α-fodrin (15). In addition, Lim *et al.* (16) identified an interaction between the ARR domain of Shank1 and Sharpin; the highly similar ARR of Shank3 was not tested in that study. We coexpressed Shank3 and Sharpin in HEK293 cells and analyzed the interaction of both proteins by precipitating Shank3 with immobilized GKAP C-terminal peptide. Use of this high affinity ligand of the Shank PDZ domain (31) for purification eliminates the need for antibodies, which in some cases interfere with the detection of proteins around 50 kDa (such as Sharpin) due to the presence of the antibody heavy chain (see Ref. 32 for a description of this method). By Western blot analysis of lysate and precipitate samples, we found that Sharpin does indeed interact with Shank3 as it could be detected in precipitates derived from Shank3-expressing cells but not from control cells in the absence of Shank3 (Fig. 3*A*). Sharpin could also be coprecipitated with all three Shank3 mutants tested. Quantitative analysis of Western blot signals showed that, based on the amount of Sharpin present in input samples, more Sharpin was coprecipitated by each of the Shank3 mutants compared with the wild type.

Similarly, we coexpressed and coprecipitated WT and mutant Shank3 variants with a GFP-tagged, C-terminal fragment of α-fodrin, which contains the site of interaction for the ARR of Shank1 and Shank3 (15). Again, the L68P and Q321R mutations slightly (but not significantly) improved binding, whereas binding of α-fodrin to the R300C mutant was slightly reduced.

Thus, all three mutations tested differentially affected the binding of ARR ligands. Interestingly, Leu-68 is located within the SPN region and is therefore outside the region directly interacting with Sharpin and α-fodrin (15, 16). The SPN region

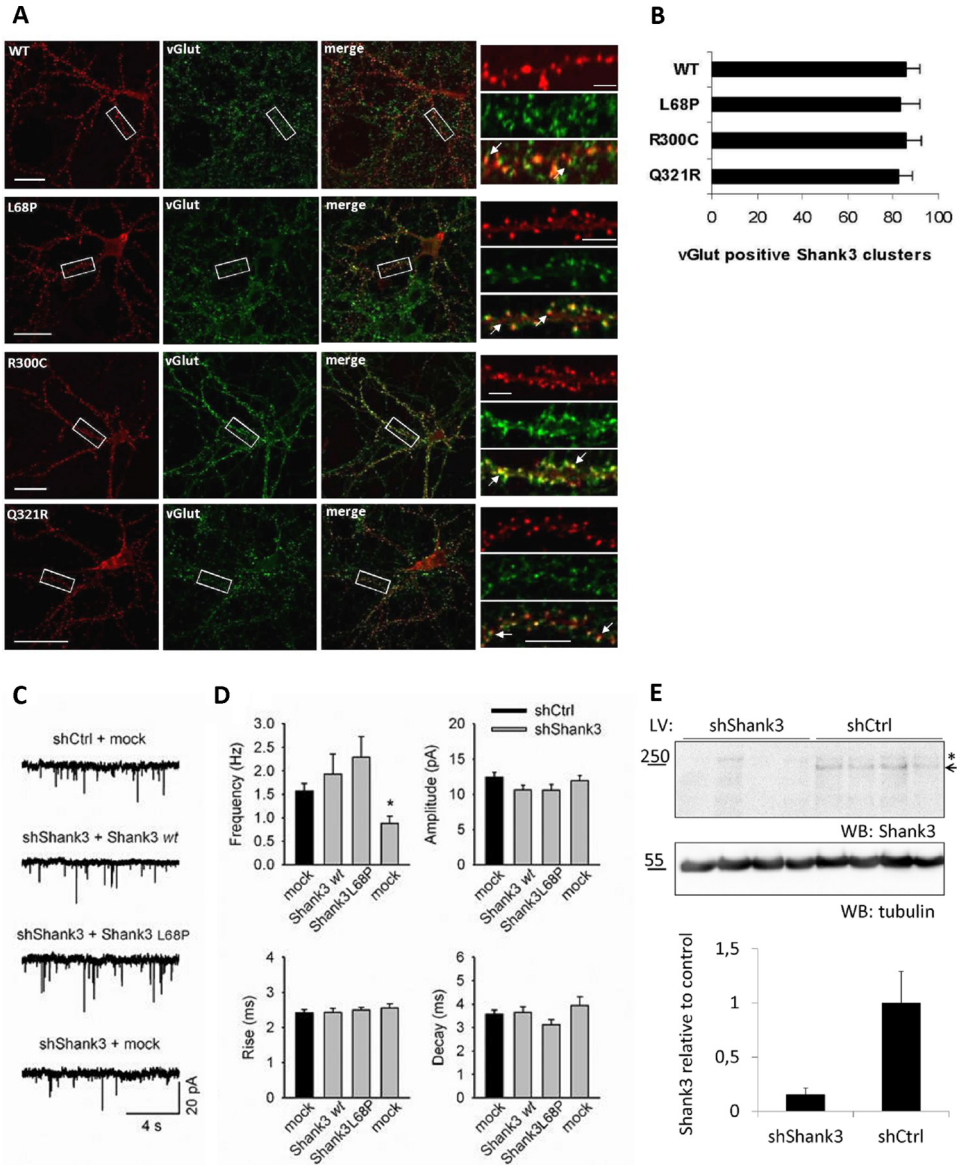

FIGURE 2. **Shank3 ASD mutants are targeted to postsynaptic sites and support normal excitatory synaptic transmission.** *A*, Shank3 expression constructs transfected into primary cultured hippocampal neurons as in Fig. 1. Neurons were fixed and stained using anti-myc (Shank3; *red fluorescence*) and anti-vGlut (a marker for glutamatergic presynaptic terminals, *green fluorescence*). Cells were visualized using confocal fluorescence microscopy. Dendritic segments indicated by *white rectangles* are shown in higher magnification; *arrows* point to Shank3- and vGlut-immunopositive clusters. *Scale bars*, 20 μm, 4 μm in magnified pictures. *B*, quantification of *A*. The percentage of Shank3 clusters with an attached vGlut immunopositive terminal (±S.D.) is depicted. 30 dendritic segments from three individual experiments were evaluated per construct. *C–E*, Shank3 expression knocked down by lentiviral shRNA in hippocampal neurons. *C*, representative mEPSCs recorded on DIV14 from control neurons (shCtrl + mock), at a holding potential of −60 mV in the presence of 0.5 μM tetrodotoxin and 50 μM picrotoxin, after knockdown of Shank3 (shShank3 + mock) at DIV8 and after transfection of Shank3 knocked down neurons with Shank3 WT and L68P mutant Shank3 at DIV11 (shShank3 + Shank3 WT and shShank3 + Shank3 L68P). *D*, summary graphs of the frequency, amplitude, rise, and decay time of mEPSCs in shCtrl + mock ($n = 13$ cells), shShank3 + Shank3 WT ($n = 9$ cells), shShank3 + Shank3 L68P ($n = 12$ cells), shShank3 + mock ($n = 16$ cells) treated groups. Data are from four independent experiments. ANOVA on ranks revealed a difference in frequency among the four groups ($p < 0.01$). The frequency of mEPSCs is decreased in shShank3 + mock-treated neurons compared with shCtrl + mock (*, $p < 0.05$, Dunn's *t* test for multiple comparisons). Data are presented as mean ± S.E. (*error bars*). *E*, Western blot (*WB*) analysis of four samples each for shShank3- and shCtrl-infected cells using anti-Shank3 and anti-tubulin antibodies revealing efficient knockdown. Shank3 signal intensity (*arrow* in *upper panel*) was normalized to tubulin signals and depicted in relation to the values derived from shCtrl-infected cells. *, position of a weak nonspecific signal above 250 kDa.

and the sequence surrounding Leu-68 are highly conserved, as shown in Fig. 4*A* (6, 33).

Intramolecular Interaction between SPN and ARR Domains—To assess the functional relevance of the SPN region, we searched for interaction partners in a yeast two-hybrid screen; the SPN of Shank1 (Shank1 amino acid residues 1–103) was used in this experiment. A screen of 20×10^6 clones of a human brain cDNA library yielded three interacting clones, only one of which passed the specificity tests of the screen. Sequence analysis showed that it contained a fragment of Shank1 cDNA fused at its 3′ end to a portion of mitochondrial DNA. The mitochondrial DNA sequence could be deleted without affecting the interaction in the yeast system (Fig. 4*B*).

The Shank1 prey clone isolated from our screen encodes amino acids 86–418 of human Shank1, thus encompassing the entire ARR of Shank1 (predicted from amino acid residues

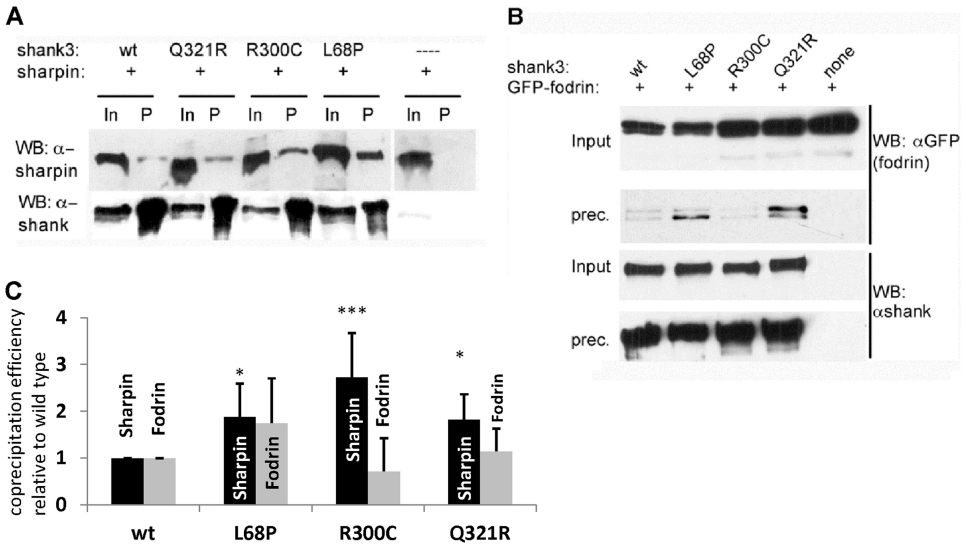

FIGURE 3. **ASD mutations facilitate binding of Shank3 to ligands of the ARR domain.** *A*, WT or mutant myc-tagged Shank3 was coexpressed with Sharpin in HEK cells. Shank3 was precipitated from cell lysates using GKAP-Sepharose. Input (*In*) and precipitate (*P*) samples were analyzed by Western blotting (*WB*) using the antibodies indicated. *B*, WT or mutant Shank3 was coexpressed with a GFP fusion protein containing the C-terminal portion of α-fodrin. Shank3 was precipitated as in *A*, and input and precipitate samples were analyzed by Western blotting. *C*, quantitation of data shown in *A* and *B*. Means ± S.D. (*error bars*) are shown. Signals of the Sharpin- (*black bars*) or α-fodrin- (*gray bars*) specific bands were quantitated, and the ratio of precipitate to input was calculated. For each experiment, this was normalized to the ratio obtained with the WT Shank3 protein. *, $p < 0.05$; ***, 0.001, significantly different from WT (ANOVA, followed by Dunnett's correction for multiple comparisons; $n = 4–5$).

107–328) and some additional C-terminal sequence. This indicates that the Shank1 SPN domain interacts with the Shank1 ARR domain. This interaction could be intramolecular within the same Shank molecule, or intermolecular, linking two or more Shank proteins in the PSD. To differentiate between these possibilities, we performed a two-hybrid assay with the SPN domain bait construct, and prey constructs containing either the ARR alone or the full N-terminal region containing SPN and ARR domains. Only yeast colonies expressing the isolated ARR domain (residues 86–418) showed a strong interaction whereas those containing the entire N-terminal region comprising SPN and ARR domains (1–418) did not (Fig. 4*B*). This was not due to different expression levels in the yeast strains used, as both the 1–418 fragment and the 86–418 fragment were produced at similar levels, whereas the 86–418+mt fragment (which strongly supported growth in selective media) was produced at rather low levels (Fig. 4*C*). These data suggest that an intramolecular interaction between SPN and ARR domains is preferred over the intermolecular interaction, to the effect that intramolecular binding blocks access of exogenous SPN domain to the ARR domain. Further support for this concept came from experiments in HEK cells where we coexpressed a GFP fusion protein of the Shank1 SPN domain with either the N-terminal half of Shank1 (SPN to PDZ domain) or the same construct lacking the SPN domain. In addition we introduced the L61P mutation, which corresponds to the L68P mutation in Shank3. Upon precipitation of Shank1 variants by GKAP-Sepharose, we observed that the SPN-GFP fusion could be co-precipitated with the WT Shank1 version, but the efficiency of coprecipitation was increased by the L61P mutation and even more so by removal of the SPN domain in the Shank1ΔSPN construct (Fig. 4, *D* and *E*). These data also indicated that the L61P mutation (or L68P in Shank3) might interfere with the inhibitory role of the SPN domain.

Similarly, the intramolecular interaction was observed in Shank3, when we coexpressed full-length Shank3 or a Shank3 deletion mutant lacking the SPN motif (Shank3ΔSPN) with the GFP-tagged SPN of Shank3. Here, the Shank3ΔSPN variant was expressed at lower levels (10–20%) compared with WT Shank3; this may be due to altered translation initiation (because of altered context of the start codon), or inefficient folding of the ARR in the absence of its interacting SPN domain. Nevertheless, we observed that more Shank3ΔSPN was coimmunoprecipitated with the GFP-SPN compared with WT Shank3 (Fig. 5*A*). Also, the increase in binding which we observed upon removal of the SPN domain was much stronger in Shank3 compared with Shank1.

To analyze whether the intramolecular interaction in Shank3 might also be affected by ASD mutations, the GFP-tagged Shank3 SPN domain was coexpressed with WT and mutant forms of full-length Shank3, followed by immunoprecipitation of GFP-SPN. The R12C mutation, which is also localized in the SPN domain, was included here. We observed that none of the Shank3 forms could be coprecipitated with GFP-SPN, with the exception of the L68P mutant which was readily detected in precipitates (Fig. 5*B*). We concluded that the SPN-ARR interaction blocks the ARR domain to the exogenously expressed SPN domain and that this blockade is relieved by the L68P mutation in the SPN. Consistently, we observed that introduction of L68P into the isolated SPN domain blocked interaction with full-length Shank3, regardless of whether this was in the WT "closed" form or in the L68P mutant "open" form. On the other hand, the R12C mutation did not interfere with the binding of the SPN domain to full-length L68P mutant Shank3 (Fig. 5*C*). These data were confirmed by a reverse experiment whereupon precipitation by GKAP-Sepharose WT and R12C mutant full-length Shank3 did not coprecipitate with the GFP-tagged

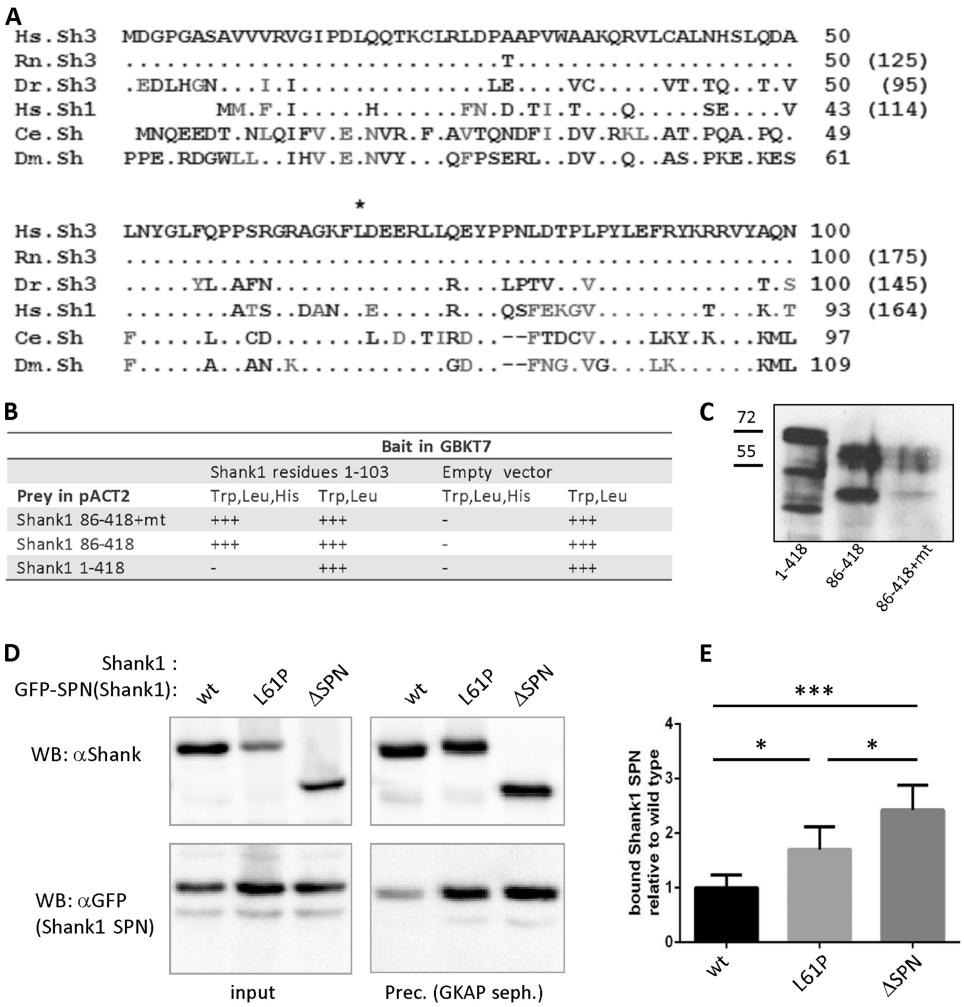

FIGURE 4. **The SPN domain of Shank1 is involved in an intramolecular interaction with the ARR domain.** *A*, sequence alignment of the first 100 residues of human Shank3 (Hs.Sh3) with Shank3 from rat (Rn.Sh3) and zebra fish (*Danio rerio*; Dr.Sh3), the single Shank proteins present in worm (*Caenorhabditis elegans*, Ce.Sh), and fly (*Drosophila melanogaster*, Dm.Sh), as well as human Shank1 (Hs.Sh1). Identical residues are indicated by *dots*, gaps by *dashes*, and conservative substitutions in *gray*. The position of Leu-68 is indicated by an *asterisk*. As described in the legend of Fig. 1, two alternative translational start sites may be used in the case of rat Shank3; the same holds true for human (and rat) Shank1, and for *D. rerio* Shank3. In these cases, *numbering* refers to the shorter variant, and the numbering for the longer variant is given in *parentheses*. *B*, results of a yeast two-hybrid screen with the SPN domain of Shank1 as a bait. The only positive clone obtained in this screen contained a cDNA fragment coding for amino acids 86–418 of human Shank1, fused to a fragment of mitochondrial DNA (*mt*). Shown is the result of a retransformation assay with the original clone, a plasmid lacking the mtDNA, and a plasmid that codes for the full N-terminal region of Shank, which includes the SPN and ARR domain. Positive signals refer to growth on Trp- and Leu-deficient media (documenting the presence of both bait and prey plasmids) or on Trp-, Leu-, and His-deficient media (documenting an efficient interaction between proteins expressed on both plasmids). Note that the SPN in the bait vector cannot bind when the SPN region is also present in the prey vector. *C*, Western blot analysis of lysates of yeast expressing the Shank1 fragments indicated, using anti-HA antibody directed against the HA tag encoded by the pACT2 prey vector. *D*, GFP fusion of the Shank1 SPN fragment coexpressed with Shank1 fragments carrying WT or L61P mutant sequence, or lacking the SPN domain (ΔSPN) as indicated. From cell lysates, Shank1 was precipitated using GKAP-Sepharose, and input (*In*) and precipitate (*P*) samples were analyzed by Western blotting (*WB*) using the antibodies indicated. *E*, the efficiency of coprecipitation of the Shank1 SPN domain was determined as in Fig. 3*C*. Data are shown as mean ± S.D. (*error bars*). (*, $p < 0.05$; ***, $p < 0.001$, ANOVA, $n = 4–5$).

WT SPN domain whereas L68P mutant Shank3 did interact efficiently (Fig. 5*D*).

Introduction of a proline, as in the L68P mutation, may often be deleterious to protein structure as proline interferes with the formation of secondary structure elements. This may apply here also, as a secondary structure prediction of the Shank3 N terminus suggests that a long helical segment around amino acid 70 is considerably shortened by the L68P mutation (Fig. 6*A*). Furthermore, as we hypothesized that the SPN domain folds back on the ARR domain we generated bacterial expression constructs coding for residues 1–99 and 1–148 (both containing the SPN domain) and 1–348 (SPN-ARR double domain). Expression of these fragments with an N-terminal His tag resulted in insoluble proteins. To enhance solubility we added an N-terminal SUMO tag to these fragments. Both 1–99 and 1–148 fragments remained insoluble as fusion proteins. However, the 1–348 double domain expressed at high levels as a soluble protein and remained in solution after removal of SUMO by cleavage with SUMO protease. The ^{1}H NMR spectrum of the Shank3(1–348) fragment (Fig. 6, *B* and *C*) shows high chemical shift dispersion and a lack of strong sharp signals or large composite peaks in the areas corresponding to unstructured polypeptides. This demonstrates that most of the residues in Shank3(1–348) are incorporated into the folded protein regions. L68P mutant Shank3(1–348), however, could not be obtained in a soluble form, suggesting that the introduction of a

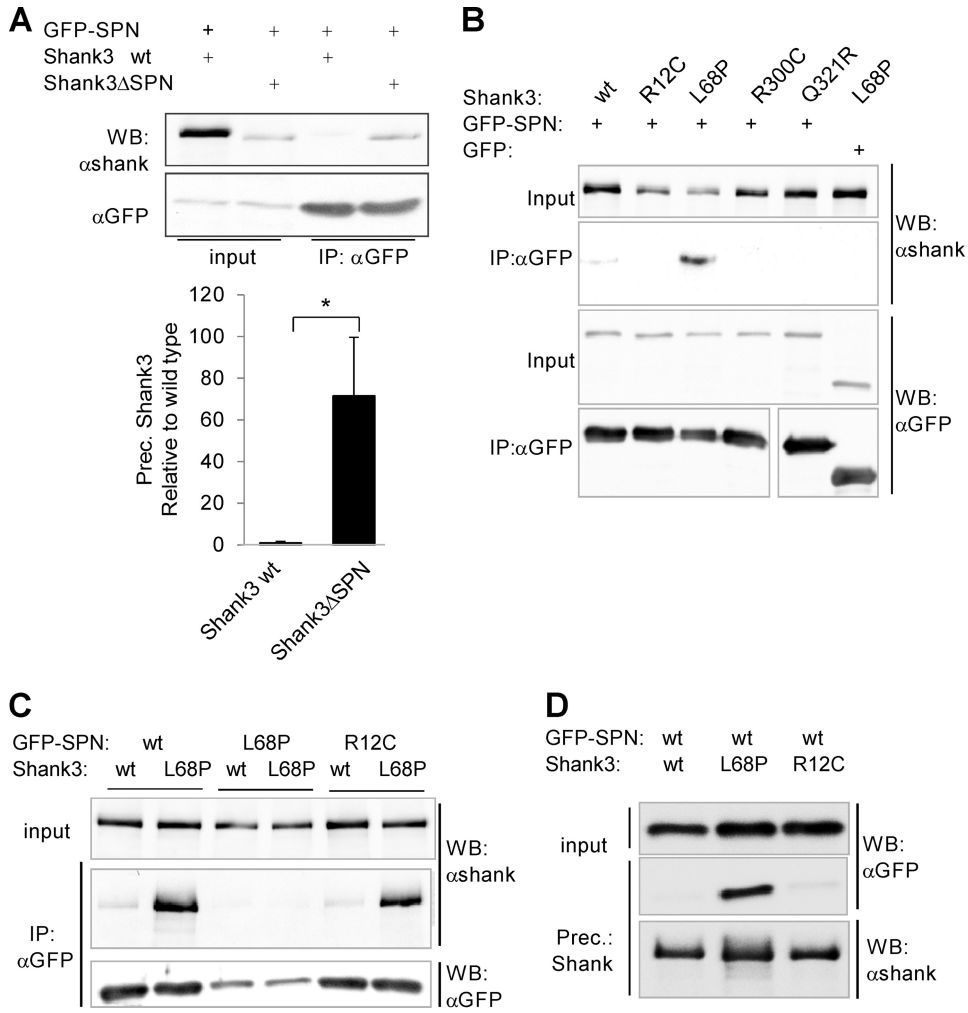

FIGURE 5. **The L68P mutation interferes with the ability of the Shank3 SPN domain to bind to the ankyrin repeat region.** *A*, a GFP fusion of the Shank3 SPN domain was coexpressed with full-length myc-tagged Shank3 or a similar construct lacking the SPN motif (Shank3ΔSPN). GFP-SPN was precipitated from cell lysates, and input and precipitate samples were analyzed by Western blotting (*WB*). Note that much more Shank3ΔSPN is coprecipitated with the SPN fragment despite its lower expression level. *, significantly different from WT, $p < 0.05$ (Student's *t* test; $n = 3$). *B*, WT and mutant full-length Shank3-myc constructs were coexpressed with a GFP fusion of the SPN domain of Shank3 (or GFP alone). GFP-containing proteins were precipitated from cell lysates, and input and precipitate samples were analyzed by Western blotting using the antibodies indicated. Note that only the L68P mutant form of Shank3 interacted with the SPN domain in this assay. *C*, WT and L68P mutant full-length Shank3 were coexpressed with WT and mutant (R12C or L68P) SPN domain fused to GFP. GFP-containing proteins were precipitated from cell lysates and analyzed as in *A*. *D*, WT and mutant full-length Shank3 were coexpressed with the WT Shank3 SPN domain fused to GFP. Shank3 was precipitated using GKAP-Sepharose; input and precipitate samples were analyzed by Western blotting.

proline at this position may indeed disrupt the secondary structure or the folding of the SPN domain.

To further compare the binding properties of Shank3 toward the three known ligands of the ARR domain, we generated a series of deletion constructs of Shank3, either as WT or as L68P mutant forms fused to the mRFP coding sequence (Fig. 7*A*). Here, the SH3 domain as well as the region between ARR and SH3 were included in some constructs, to determine whether they also affect the function of the ARR. Sharpin, a fragment of α-fodrin, and the Shank SPN domain were expressed as GFP fusion proteins, and interaction was analyzed by immunoprecipitation of either GFP fusion proteins or the mRFP-tagged Shank fusion proteins (Fig. 7, *B–E*). We observed for all three ARR ligands that their interaction with Shank3 was strongly enhanced by the L68P mutation. In addition, α-fodrin, SPN, and Sharpin required the ARR domain but no additional elements of the Shank3 sequence for binding, as interaction was observed in each case when the isolated ARR was used. A difference between the ARR ligands was observed only with one construct (Shank3(75–376), containing approximately 30 residues C-terminal to the ARR domain) which did not bind to Sharpin, interacted weakly with α-fodrin, and strongly with the SPN domain.

DISCUSSION

It is generally understood that haploinsufficiency of the *SHANK3* gene causes mental illness, either manifest as intellectual disability in case of the 22q13 deletion syndrome (34) or as autism (3). Gene targeting studies in mice confirmed the role of both Shank3 and Shank2 for the development of an autistic phenotype (35–38). In humans, larger deletions within the *SHANK3* gene or truncating mutations have been observed which are consistent with a loss of function of one copy of the gene. In the case of point mutations which have been found in several autistic patients, the functional significance of these changes remains rather unclear for several reasons. Most muta-

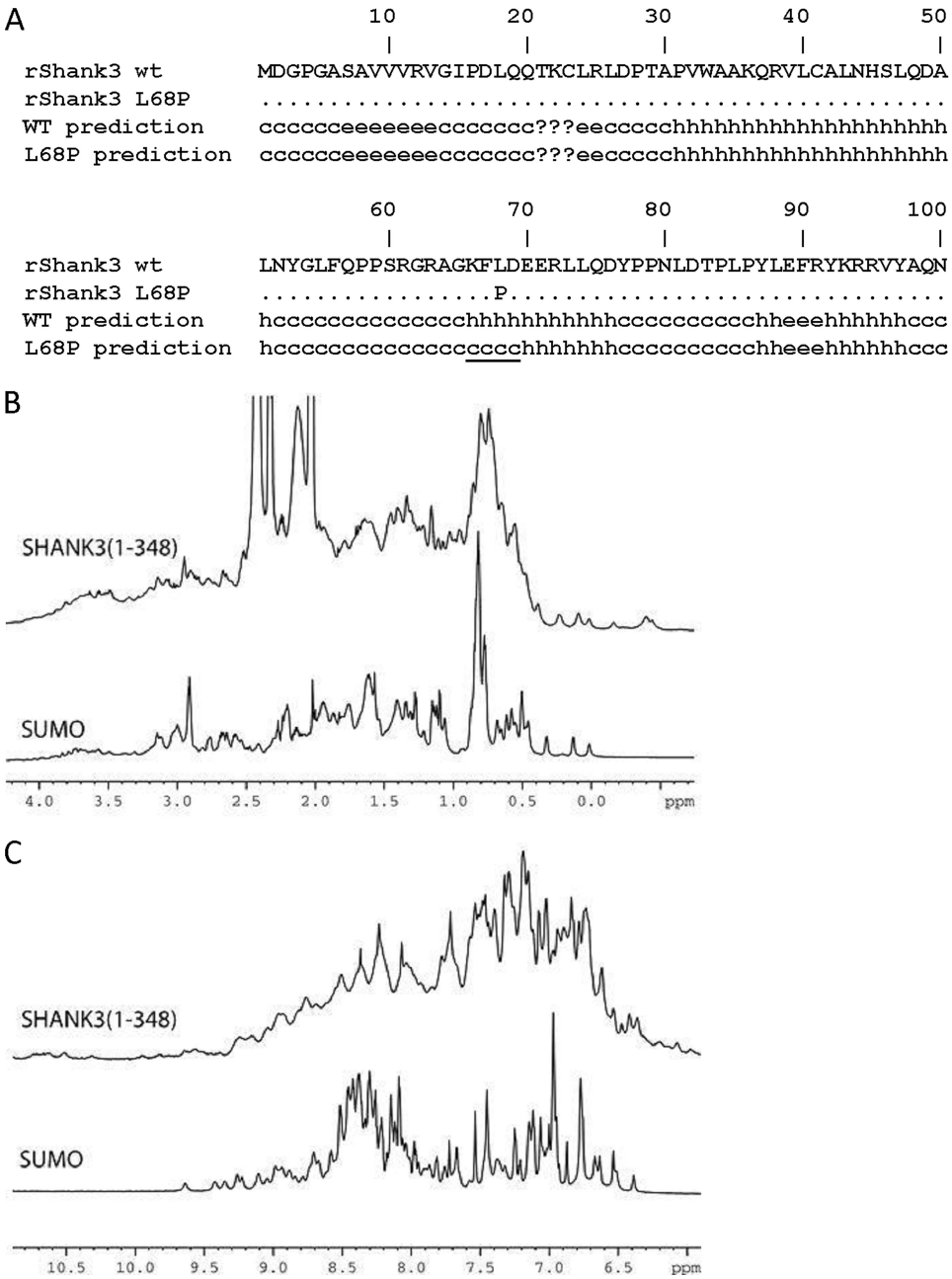

FIGURE 6. **Structural analysis of Shank3 SPN region.** *A*, secondary structure prediction for the first 100 amino acids of rat Shank3 and its L68P mutant; *h*, α-helical; *e*, extended; *c*, random coil; ?, ambiguous. Note that the L68P mutation is predicted to disrupt a long α-helical stretch around amino acid 70. The lost helical part is *underlined*. *B* and *C*, ^{1}H NMR 800-MHz spectra of Shank3(1–348) (*top*) and SUMO (*bottom*). High field aliphatic region (*B*) and low field amide region (*C*) are shown separately for clarity. High chemical shift dispersion and lack of sharp intense signals demonstrate that both SPN and ARR domains are folded, and the Shank3(1–348) does not include extensive unstructured regions. All Shank3(1–348) signals have similar line width and are much broader than the signals of SUMO, which has a size similar to that of the SPN domain. This suggests that SPN and ARR domains make a close contact and move as integrated unit.

tions lead to changes in those parts of the protein, which are not required for synaptic targeting of Shank proteins and do not contribute to the enhanced formation of dendritic spines, which has been observed under conditions of Shank overexpression (10, 11, 39). Furthermore, it is not known whether these mutations affect interactions with identified binding partners of Shank proteins.

In this study, we analyzed several mutations which are localized within the N-terminal segment of Shank3 (SPN + ARR). We established by biochemical assays that the mutations differentially affect binding to Sharpin, and α-fodrin, the two known ligands of the ARR domain. Interestingly, enhanced binding was observed with the L68P mutation which is not located in the ARR domain, but within the SPN domain of Shank3. Our subsequent analyses by yeast two-hybrid assays and the expression of deletion constructs showed that the SPN region constitutes a novel functional domain of Shank proteins which has so far been overlooked. We observe here that the SPN is involved in an intramolecular, inhibitory interaction with the ARR.

Our NMR analysis further supports the notion that both SPN and ARR domains are folded and either connected by a very

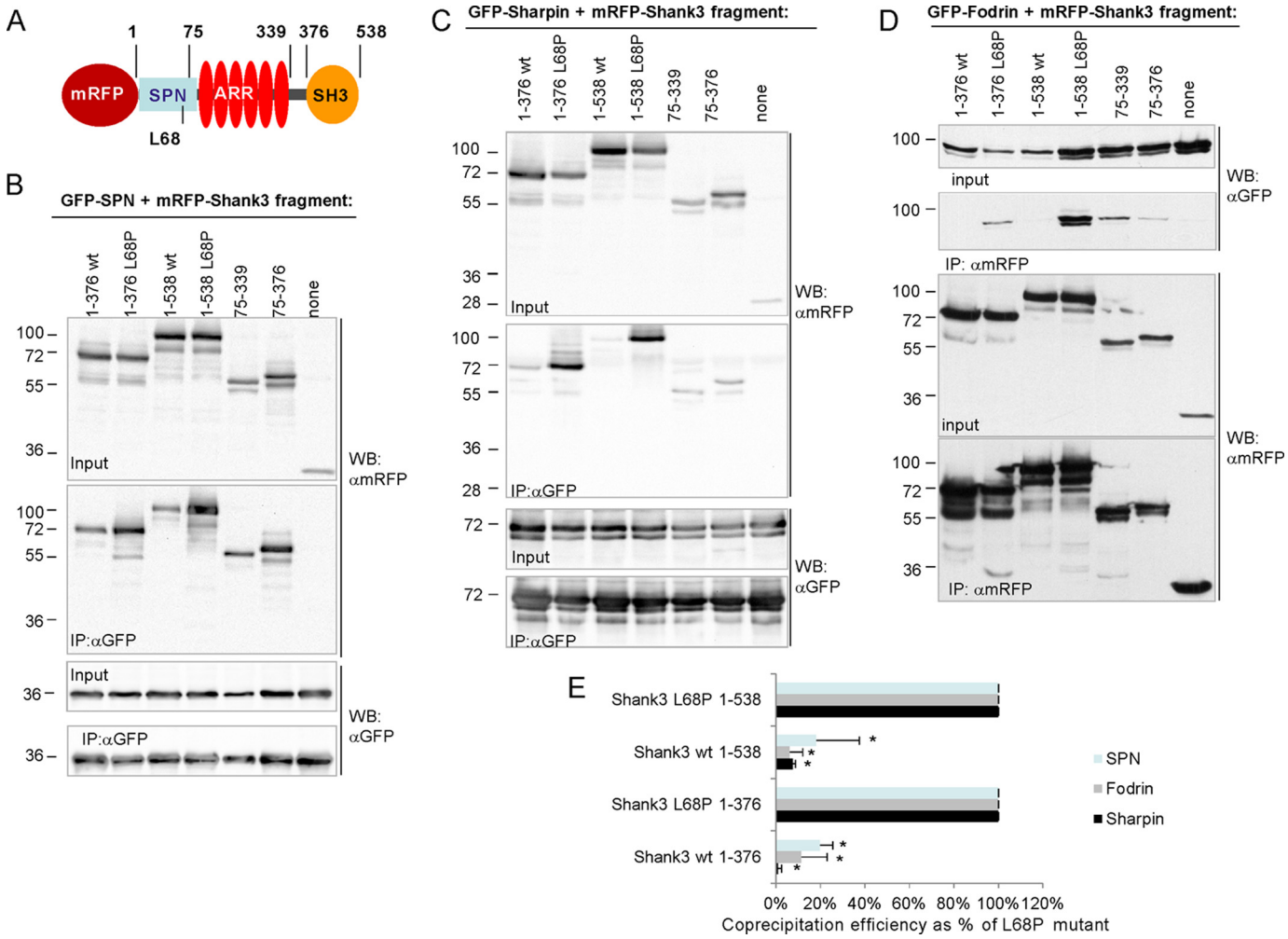

FIGURE 7. **All ligands of the Shank3 ARR are similarly affected by the L68P mutation.** *A*, overview shows positions in the N-terminal part of Shank3, which were used to generate WT and L68P mutant deletion constructs of Shank3 fused to mRFP, as indicated. *B–D*, constructs were coexpressed with GFP-tagged SPN domain (*B*), Sharpin (*C*), or α-fodrin C-terminal domain (*D*). After cell lysis and precipitation of tagged proteins via GFP trap (*B* and *C*) or mRFP trap (*D*) matrices, input and immunoprecipitated (*IP*) samples were analyzed by Western blotting (*WB*) using anti-GFP and anti-mRFP antibodies. Note that in each case the L68P mutation strongly facilitates binding to the ARR domain. As shown in Fig. 3 for Shank1, binding of SPN-containing Shank3 is also significantly reduced compared with Shank3 fragments not containing the SPN region. *E*, effect of the L68P mutant on binding to different ARR ligands is quantified. The ratio of precipitate to input signal was determined for coprecipitated proteins; data were then normalized to the value obtained with the L68P mutant construct (set as 100% in the figure). Means ± S.D. (*error bars*) are shown. *, WT significantly different from L68P mutant, $p < 0.05$, Students *t* test; $n = 3–4$.

short linker or a linker that is structured and immobilized in the SPN-ARR double domain. All the signals in isolated Shank3(1–348) have uniform line width that is much larger than the line width in small globular proteins of a similar size to the SPN domain, such as SUMO. These characteristics indicate that SPN and ARR domains make a stable contact and move as a single unit. In the absence of interdomain interaction the relative motion of the domains would strongly reduce the line width of signals from the smaller SPN domain and make these signals comparable with the signals of a small protein of a similar size. Although we do not have resonance assignments for Shank3(1–348), the signals with reduced line width would be easily identifiable in the one-dimensional spectra. The lack of a flexible linker between the domains and uniformly broadened resonances suggests association of the SPN and ARR domains. This is indirectly supported by the aggregation of the isolated SPN domain that may be caused by the exposure of the residues that make contact with the ARR domain.

In a cellular system, the binding of the SPN domain prevents access of both α-fodrin and Sharpin to the ARR. The isolated SPN domain exhibits similar binding properties compared with α-fodrin and Sharpin. Differences between ARR ligands were observed with one Shank3 fragment only (residues 75–376) which did not bind to Sharpin but did bind to SPN and α-fodrin. The reasons for this discrepancy are unclear, but these results may point to additional regulatory mechanisms within the Shank3 protein. We conclude that all three ligands of the ARR compete for the same binding interface. Blocking access to a specific domain through intramolecular interactions is a mechanism frequently employed to place this domain under regulatory control within a cellular signaling pathway. Our data suggest that regulated access to the Shank3 ARR by the SPN domain carries functional relevance in intracellular signaling.

It should be noted here that both the SPN and the ARR domains are highly conserved throughout evolution and can be

detected in all known Shank proteins (33), including Shank variants identified in nerveless, unicellular organisms such as choanoflagellates (33). As pointed out by Gauthier *et al.* (6), the sequence around Leu-68 is particularly well conserved. This part is predicted to be α-helical, and disruption of this helical segment by introduction of a proline may cause misfolding of the SPN domain. In agreement, we were unable to produce soluble Shank3(1–348) protein carrying the L68P mutation.

Splice and promoter variants of Shank1–3 exist which do not contain both the SPN and ARR domains (14); thus the Shank2 forms expressed in the forebrain lack this region (37). However, no variant has been identified which contains only one of the two domains. Thus we believe that the SPN-ARR linkage is an element of a physiologically relevant regulatory circuit controlling ARR function. Regulation of this circuit appears to be more tight for Shank3 than for Shank1, as removal of the SPN domain has a stronger effect in Shank3 than in Shank1 (Figs. 4*E* and 5*A*). Importantly, the L68P mutation detected in an autistic patient disrupts this circuit and leaves the ARR domain in a permanently open state allowing for unregulated access of ligands. Consequently, the L68P mutation should be considered a gain-of-function mutation, which allows the mutant Shank3 protein to bind better and possibly also prematurely to its interacting partners.

Our electrophysiological analysis further supports the notion that L68P mutant Shank3 is not a loss-of-function mutant. Knockdown of endogenous Shank3 expression in cultured neurons led to a reduced frequency of mEPSCs, consistent with the role described for Shank3 in synapse formation (10, 11). Miniature EPSP frequency could be rescued by reexpression of either WT or mutant Shank3 in a similar manner. Further work will be required to elucidate the molecular mechanisms by which an enhanced interaction of the ARR with either α-fodrin or Sharpin may contribute to the pathology of autism. The increased interaction of the ARR with α-fodrin observed with the L68P mutation may be involved in the dysregulation of the actin cytoskeleton of the dendritic spine, as has been described in the case of R300C and Q321R mutants (13). Interestingly, Sharpin has recently been described as a component of the E3 ubiquitin ligase complex which is involved in assembly of linear ubiquitin chains and plays a role in TNFα signaling in nonneuronal cells (17–19). Thus postsynaptic signal transduction may be altered in neurons carrying the L68P mutant form of Shank3.

REFERENCES

1. Autism Genome Project Consortium, Szatmari, P., Paterson, A. D., Zwaigenbaum, L., Roberts, W., Brian, J., Liu, X. Q., Vincent, J. B., Skaug, J. L., Thompson, A. P., Senman, L., Feuk, L., Qian, C., Bryson, S. E., Jones, M. B., Marshall, C. R., Scherer, S. W., Vieland, V. J., Bartlett, C., Mangin, L. V., Goedken, R., Segre, A., Pericak-Vance, M. A., Cuccaro, M. L., Gilbert, J. R., Wright, H. H., Abramson, R. K., Betancur, C., Bourgeron, T., Gillberg, C., Leboyer, M., Buxbaum, J. D., Davis, K. L., Hollander, E., Silverman, J. M., Hallmayer, J., Lotspeich, L., Sutcliffe, J. S., Haines, J. L., Folstein, S. E., Piven, J., Wassink, T. H., Sheffield, V., Geschwind, D. H., Bucan, M., Brown, W. T., Cantor, R. M., Constantino, J. N., Gilliam, T. C., Herbert, M., Lajonchere, C., Ledbetter, D. H., Lese-Martin, C., Miller, J., Nelson, S., Samango-Sprouse, C. A., Spence, S., State, M., Tanzi, R. E., Coon, H., Dawson, G., Devlin, B., Estes, A., Flodman, P., Klei, L., McMahon, W. M., Minshew, N., Munson, J., Korvatska, E., Rodier, P. M., Schellenberg, G. D., Smith, M., Spence, M. A., Stodgell, C., Tepper, P. G., Wijsman, E. M., Yu, C. E., Roge, B., Mantoulan, C., Wittemeyer, K., Poustka, A., Felder, B., Klauck, S. M., Schuster, C., Poustka, F., Bolte, S., Feineis-Matthews, S., Herbrecht, E., Schmotzer, G., Tsiantis, J., Papanikolaou, K., Maestrini, E., Bacchelli, E., Blasi, F., Carone, S., Toma, C., Van Engeland, H., de Jonge, M., Kemner, C., Koop, F., Langemeijer, M., Hijmans, C., Staal, W. G., Baird, G., Bolton, P. F., Rutter, M. L., Weisblatt, E., Green, J., Aldred, C., Wilkinson, J. A., Pickles, A., Le Couteur, A., Berney, T., McConachie, H., Bailey, A. J., Francis, K., Honeyman, G., Hutchinson, A., Parr, J. R., Wallace, S., Monaco, A. P., Barnby, G., Kobayashi, K., Lamb, J. A., Sousa, I., Sykes, N., Cook, E. H., Guter, S. J., Leventhal, B. L., Salt, J., Lord, C., Corsello, C., Hus, V., Weeks, D. E., Volkmar, F., Tauber, M., Fombonne, E., Shih, A., and Meyer, K. J. (2007) Mapping autism risk loci using genetic linkage and chromosomal rearrangements. *Nat. Genet.* **39,** 319–328
2. Jamain, S., Quach, H., Betancur, C., Råstam, M., Colineaux, C., Gillberg, I. C., Soderstrom, H., Giros, B., Leboyer, M., Gillberg, C., Bourgeron, T., Paris Autism Research International Sibpair Study (2003) Mutations of the X-linked genes encoding neuroligins NLGN3 and NLGN4 are associated with autism. *Nat. Genet.* **34,** 27–29
3. Durand, C. M., Betancur, C., Boeckers, T. M., Bockmann, J., Chaste, P., Fauchereau, F., Nygren, G., Rastam, M., Gillberg, I. C., Anckarsäter, H., Sponheim, E., Goubran-Botros, H., Delorme, R., Chabane, N., Mouren-Simeoni, M. C., de Mas, P., Bieth, E., Rogé, B., Héron, D., Burglen, L., Gillberg, C., Leboyer, M., and Bourgeron, T. (2007) Mutations in the gene encoding the synaptic scaffolding protein SHANK3 are associated with autism spectrum disorders. *Nat. Genet.* **39,** 25–27
4. Sato, D., Lionel, A. C., Leblond, C. S., Prasad, A., Pinto, D., Walker, S., O'Connor, I., Russell, C., Drmic, I. E., Hamdan, F. F., Michaud, J. L., Endris, V., Roeth, R., Delorme, R., Huguet, G., Leboyer, M., Rastam, M., Gillberg, C., Lathrop, M., Stavropoulos, D. J., Anagnostou, E., Weksberg, R., Fombonne, E., Zwaigenbaum, L., Fernandez, B. A., Roberts, W., Rappold, G. A., Marshall, C. R., Bourgeron, T., Szatmari, P., and Scherer, S. W. (2012) *SHANK1* deletions in males with autism spectrum disorder. *Am. J. Hum. Genet.* **90,** 879–887
5. Berkel, S., Marshall, C. R., Weiss, B., Howe, J., Roeth, R., Moog, U., Endris, V., Roberts, W., Szatmari, P., Pinto, D., Bonin, M., Riess, A., Engels, H., Sprengel, R., Scherer, S. W., and Rappold, G. A. (2010) Mutations in the *SHANK2* synaptic scaffolding gene in autism spectrum disorder and mental retardation. *Nat. Genet.* **42,** 489–491
6. Gauthier, J., Spiegelman, D., Piton, A., Lafrenière, R. G., Laurent, S., St-Onge, J., Lapointe, L., Hamdan, F. F., Cossette, P., Mottron, L., Fombonne, E., Joober, R., Marineau, C., Drapeau, P., and Rouleau, G. A. (2009) Novel *de novo SHANK3* mutation in autistic patients. *Am. J. Med. Genet. B Neuropsychiatr. Genet.* **150B,** 421–424
7. Sheng, M., and Kim, E. (2000) The Shank family of scaffold proteins. *J. Cell Sci.* **113,** 1851–1856
8. Kreienkamp, H. J. (2008) Scaffolding proteins at the postsynaptic density: Shank as the architectural framework. *Handb. Exp. Pharmacol.* 365–380
9. Boeckers, T. M., Bockmann, J., Kreutz, M. R., and Gundelfinger, E. D. (2002) ProSAP/Shank proteins: a family of higher order organizing molecules of the postsynaptic density with an emerging role in human neurological disease. *J. Neurochem.* **81,** 903–910
10. Sala, C., Piëch, V., Wilson, N. R., Passafaro, M., Liu, G., and Sheng, M. (2001) Regulation of dendritic spine morphology and synaptic function by Shank and Homer. *Neuron* **31,** 115–130
11. Roussignol, G., Ango, F., Romorini, S., Tu, J. C., Sala, C., Worley, P. F., Bockaert, J., and Fagni, L. (2005) Shank expression is sufficient to induce functional dendritic spine synapses in aspiny neurons. *J. Neurosci.* **25,** 3560–3570
12. Baron, M. K., Boeckers, T. M., Vaida, B., Faham, S., Gingery, M., Sawaya, M. R., Salyer, D., Gundelfinger, E. D., and Bowie, J. U. (2006) An architectural framework that may lie at the core of the postsynaptic density. *Science* **311,** 531–535
13. Durand, C. M., Perroy, J., Loll, F., Perrais, D., Fagni, L., Bourgeron, T., Montcouquiol, M., and Sans, N. (2012) *SHANK3* mutations identified in autism lead to modification of dendritic spine morphology via an actin-dependent mechanism. *Mol. Psychiatry* **17,** 71–84
14. Lim, S., Naisbitt, S., Yoon, J., Hwang, J. I., Suh, P. G., Sheng, M., and Kim,

E. (1999) Characterization of the Shank family of synaptic proteins: multiple genes, alternative splicing, and differential expression in brain and development. *J. Biol. Chem.* **274,** 29510–29518
15. Böckers, T. M., Mameza, M. G., Kreutz, M. R., Bockmann, J., Weise, C., Buck, F., Richter, D., Gundelfinger, E. D., and Kreienkamp, H. J. (2001) Synaptic scaffolding proteins in rat brain: ankyrin repeats of the multidomain Shank protein family interact with the cytoskeletal protein α-fodrin. *J. Biol. Chem.* **276,** 40104–40112
16. Lim, S., Sala, C., Yoon, J., Park, S., Kuroda, S., Sheng, M., and Kim, E. (2001) Sharpin, a novel postsynaptic density protein that directly interacts with the shank family of proteins. *Mol. Cell. Neurosci.* **17,** 385–397
17. Ikeda, F., Deribe, Y. L., Skånland, S. S., Stieglitz, B., Grabbe, C., Franz-Wachtel, M., van Wijk, S. J., Goswami, P., Nagy, V., Terzic, J., Tokunaga, F., Androulidaki, A., Nakagawa, T., Pasparakis, M., Iwai, K., Sundberg, J. P., Schaefer, L., Rittinger, K., Macek, B., and Dikic, I. (2011) SHARPIN forms a linear ubiquitin ligase complex regulating NF-κB activity and apoptosis. *Nature* **471,** 637–641
18. Tokunaga, F., Nakagawa, T., Nakahara, M., Saeki, Y., Taniguchi, M., Sakata, S., Tanaka, K., Nakano, H., and Iwai, K. (2011) SHARPIN is a component of the NF-κB-activating linear ubiquitin chain assembly complex. *Nature* **471,** 633–636
19. Gerlach, B., Cordier, S. M., Schmukle, A. C., Emmerich, C. H., Rieser, E., Haas, T. L., Webb, A. I., Rickard, J. A., Anderton, H., Wong, W. W., Nachbur, U., Gangoda, L., Warnken, U., Purcell, A. W., Silke, J., and Walczak, H. (2011) Linear ubiquitination prevents inflammation and regulates immune signalling. *Nature* **471,** 591–596
20. Seymour, R. E., Hasham, M. G., Cox, G. A., Shultz, L. D., Hogenesch, H., Roopenian, D. C., and Sundberg, J. P. (2007) Spontaneous mutations in the mouse *Sharpin* gene result in multiorgan inflammation, immune system dysregulation and dermatitis. *Genes Immun.* **8,** 416–421
21. Rantala, J. K., Pouwels, J., Pellinen, T., Veltel, S., Laasola, P., Mattila, E., Potter, C. S., Duffy, T., Sundberg, J. P., Kallioniemi, O., Askari, J. A., Humphries, M. J., Parsons, M., Salmi, M., and Ivaska, J. (2011) SHARPIN is an endogenous inhibitor of β1-integrin activation. *Nat. Cell Biol.* **13,** 1315–1324
22. Boeckers, T. M., Winter, C., Smalla, K. H., Kreutz, M. R., Bockmann, J., Seidenbecher, C., Garner, C. C., and Gundelfinger, E. D. (1999) Proline-rich synapse-associated proteins ProSAP1 and ProSAP2 interact with synaptic proteins of the SAPAP/GKAP family. *Biochem. Biophys. Res. Commun.* **264,** 247–252
23. Falley, K., Schütt, J., Iglauer, P., Menke, K., Maas, C., Kneussel, M., Kindler, S., Wouters, F. S., Richter, D., and Kreienkamp, H. J. (2009) Shank1 mRNA: dendritic transport by kinesin and translational control by the 5′-untranslated region. *Traffic* **10,** 844–857
24. Campbell, R. E., Tour, O., Palmer, A. E., Steinbach, P. A., Baird, G. S., Zacharias, D. A., and Tsien, R. Y. (2002) A monomeric red fluorescent protein. *Proc. Natl. Acad. Sci. U.S.A.* **99,** 7877–7882
25. Zitzer, H., Hönck, H. H., Bächner, D., Richter, D., and Kreienkamp, H. J. (1999) Somatostatin receptor interacting protein defines a novel family of multidomain proteins present in human and rodent brain. *J. Biol. Chem.* **274,** 32997–33001
26. Dityatev, A., Dityateva, G., and Schachner, M. (2000) Synaptic strength as a function of post- *versus* presynaptic expression of the neural cell adhesion molecule NCAM. *Neuron* **26,** 207–217
27. Jiang, M., and Chen, G. (2006) High Ca^{2+}-phosphate transfection efficiency in low-density neuronal cultures. *Nat. Protoc.* **1,** 695–700
28. Moult, P. R., Gladding, C. M., Sanderson, T. M., Fitzjohn, S. M., Bashir, Z. I., Molnar, E., and Collingridge, G. L. (2006) Tyrosine phosphatases regulate AMPA receptor trafficking during metabotropic glutamate receptor-mediated long-term depression. *J. Neurosci.* **26,** 2544–2554
29. Combet, C., Blanchet, C., Geourjon, C., and Deléage, G. (2000) NPS@: network protein sequence analysis. *Trends Biochem. Sci.* **25,** 147–150
30. Verpelli, C., Dvoretskova, E., Vicidomini, C., Rossi, F., Chiappalone, M., Schoen, M., Di Stefano, B., Mantegazza, R., Broccoli, V., Böckers, T. M., Dityatev, A., and Sala, C. (2011) Importance of Shank3 protein in regulating metabotropic glutamate receptor 5 (mGluR5) expression and signaling at synapses. *J. Biol. Chem.* **286,** 34839–34850
31. Naisbitt, S., Kim, E., Tu, J. C., Xiao, B., Sala, C., Valtschanoff, J., Weinberg, R. J., Worley, P. F., and Sheng, M. (1999) Shank, a novel family of postsynaptic density proteins that binds to the NMDA receptor/PSD-95/GKAP complex and cortactin. *Neuron* **23,** 569–582
32. Brendel, C., Rehbein, M., Kreienkamp, H. J., Buck, F., Richter, D., and Kindler, S. (2004) Characterization of Staufen 1 ribonucleoprotein complexes. *Biochem. J.* **384,** 239–246
33. Alié, A., and Manuel, M. (2010) The backbone of the post-synaptic density originated in a unicellular ancestor of choanoflagellates and metazoans. *BMC Evol. Biol.* **10,** 34
34. Bonaglia, M. C., Giorda, R., Borgatti, R., Felisari, G., Gagliardi, C., Selicorni, A., and Zuffardi, O. (2001) Disruption of the *ProSAP2* gene in a t(12;22)(q24.1;q13.3) is associated with the 22q13.3 deletion syndrome. *Am. J. Hum. Genet.* **69,** 261–268
35. Wang, X., McCoy, P. A., Rodriguiz, R. M., Pan, Y., Je, H. S., Roberts, A. C., Kim, C. J., Berrios, J., Colvin, J. S., Bousquet-Moore, D., Lorenzo, I., Wu, G., Weinberg, R. J., Ehlers, M. D., Philpot, B. D., Beaudet, A. L., Wetsel, W. C., and Jiang, Y. H. (2011) Synaptic dysfunction and abnormal behaviors in mice lacking major isoforms of Shank3. *Hum. Mol. Genet.* **20,** 3093–3108
36. Peça, J., Feliciano, C., Ting, J. T., Wang, W., Wells, M. F., Venkatraman, T. N., Lascola, C. D., Fu, Z., and Feng, G. (2011) Shank3 mutant mice display autistic-like behaviours and striatal dysfunction. *Nature* **472,** 437–442
37. Schmeisser, M. J., Ey, E., Wegener, S., Bockmann, J., Stempel, A. V., Kuebler, A., Janssen, A. L., Udvardi, P. T., Shiban, E., Spilker, C., Balschun, D., Skryabin, B. V., Dieck, S., Smalla, K. H., Montag, D., Leblond, C. S., Faure, P., Torquet, N., Le Sourd, A. M., Toro, R., Grabrucker, A. M., Shoichet, S. A., Schmitz, D., Kreutz, M. R., Bourgeron, T., Gundelfinger, E. D., and Boeckers, T. M. (2012) Autistic-like behaviours and hyperactivity in mice lacking ProSAP1/Shank2. *Nature* **486,** 256–260
38. Bozdagi, O., Sakurai, T., Papapetrou, D., Wang, X., Dickstein, D. L., Takahashi, N., Kajiwara, Y., Yang, M., Katz, A. M., Scattoni, M. L., Harris, M. J., Saxena, R., Silverman, J. L., Crawley, J. N., Zhou, Q., Hof, P. R., and Buxbaum, J. D. (2010) Haploinsufficiency of the autism-associated *Shank3* gene leads to deficits in synaptic function, social interaction, and social communication. *Mol. Autism* **1,** 15
39. Boeckers, T. M., Liedtke, T., Spilker, C., Dresbach, T., Bockmann, J., Kreutz, M. R., and Gundelfinger, E. D. (2005) C-terminal synaptic targeting elements for postsynaptic density proteins ProSAP1/Shank2 and ProSAP2/Shank3. *J. Neurochem.* **92,** 519–524